First ultraviolet absorption band of methane: An *ab initio* study

Rob van Harrevelt
Theoretical Chemistry, Institute for Molecules and Materials, Radboud Universiteit Nijmegen, Toernooiveld 1, 6525 ED Nijmegen, The Netherlands

(Received 13 April 2007; accepted 25 April 2007; published online 30 May 2007)

Quantum mechanical calculations of the cross sections for photodissociation of CH_4 and CD_4 in the $1t_2 \rightarrow 3s$ band are presented. The potential energy surfaces for the three states correlating with the $1\ ^1T_2$ state at tetrahedral geometries are calculated. The elements of the (3×3) matrix representing the electronic Hamiltonian in the diabatic basis are expanded in powers of nuclear coordinates, up to the second order. The expansion coefficients are based on accurate multireference configuration interaction calculations. The electronically nonadiabatic dynamics is treated with the multiconfiguration time-dependent Hartree approach. All nine internal degrees of methane are included in the quantum dynamics simulations. The calculated cross section agrees well with experiment. Semiclassical calculations using the reflection principle suggest that the peaks in the spectrum correspond to the three adiabatic electronic states correlating with the $1\ ^1T_2$ state at T_d geometries. However, the non-Born-Oppenheimer terms in the Hamiltonian have a strong effect on the positions of the peaks in the absorption spectrum. The results of semiclassical calculations, which neglect these terms, are therefore quite different from the accurate quantum results and experiment. © *2007 American Institute of Physics*. [DOI: 10.1063/1.2741551]

I. INTRODUCTION

The ultraviolet absorption spectrum of methane in the 8.8–11.4 eV photon energy range has been assigned to a $1t_2 \rightarrow 3s$ Rydberg transition.[1] The spectrum in this range shows two diffuse broad bands, centered at 9.7 and 10.4 eV. The absence of a clear vibrational progression suggests that the molecule dissociates rapidly. This is also made plausible by several *ab initio* studies of photodissociation pathways.[2–7] Experiments[1,8–11] have identified the different photofragments predicted by the calculations.

The two broad bands have generally been attributed to two Jahn-Teller components.[1,12] At tetrahedral geometries the first excited state ($1\ ^1T_2$) is threefold degenerate. Vibrations of e or t_2 symmetry lift the degeneracy. Thus, three potential energy surfaces intersect at tetrahedral geometries. For the simpler case of an excitation to a doubly degenerate excited state, Sturge[13] has discussed the shape of the absorption spectrum. Using the semiclassical Franck-Condon picture, he explained how a broad absorption band is split into two bands for excitation from a nondegenerate ground state to an E state. The band maxima correspond to vertical transitions from the ground state to the two adiabatic excited state energy surfaces. For methane, no potential energy surface for the excited state is available, and the assignment of the peaks in the spectrum to Jahn-Teller components remains uncertain. The interpretation of the double-peak feature in terms of Jahn-Teller components has been questioned by Mebel *et al.*[6] on the basis of *ab initio* calculations.

While the excited state potential energy surface for CH_4 has not yet been calculated, Dixon[14] and Frey and Davidson[15] have constructed three-valued potential energy surfaces for the CH_4^+ ion, for the three states correlating with the $1\ ^2T_2$ state at the ground state equilibrium geometry of CH_4. Their surfaces are based on a second order expansion in displacements from a tetrahedral reference geometry. Dixon[14] has examined the effect of the e and t_2 vibrations on the photoelectron spectrum using a semiclassical model. The photoelectron spectrum[16] has a similar shape as the photodissociation spectrum. The three broad bands are attributed to the three Jahn-Teller components.[16] The semiclassical calculations of Dixon[14] confirm this picture. However, the semiclassical calculations neglect the non-Born-Oppenheimer terms in the Hamiltonian, and can therefore be only qualitative.[13] These nonadiabatic terms can be very important for geometries close to intersections of the potential energy surfaces.

The aim of the present work is to calculate the cross sections for the photodissociation of methane and CD_4 in the $1t_2 \rightarrow 3s$ band. A three-valued potential energy surface is constructed following the approach of Dixon.[14] This approach yields an accurate description of the potential energy surfaces and electronically nonadiabatic couplings in the Franck-Condon region. Full dimensional quantum dynamics calculations are performed using the multiconfiguration time-dependent Hartree[17–21] (MCTDH) approach. The calculated cross section is compared with experiment,[1] and with the results of the semiclassical approach. The effect of the various vibrations on the shape of the spectrum is also analyzed.

II. THEORY

To describe the potential energy surface in the region around the ground state geometry, it is convenient to expand the electronic Hamiltonian in powers of nuclear displacements. Several authors have already applied this method to

TABLE I. Symmetry-adapted quadratic, cubic, and quartic functions of internal coordinates. Products of s_{4i} coordinates are not included. The expressions are identical to the corresponding expressions for s_{3i}. In all equations in this table, "3" can be interchanged with "4."

$(22\|a_1)=s_{2a}^2+s_{2b}^2$	$(23\|t2,x)=(-\frac{1}{2}s_{2a}+(\sqrt{3}/2)s_{2b})s_{3x}$
$(33\|a_1)=s_{3x}^2+s_{3y}^2+s_{3z}^2$	$(23\|t2,y)=(-\frac{1}{2}s_{2a}-(\sqrt{3}/2)s_{2b})s_{3y}$
$(34\|a_1)=s_{3x}s_{4x}+s_{3y}s_{4y}+s_{3z}s_{4z}$	$(23\|t2,z)=s_{2a}s_{3z}$
$(222\|a_1)=s_{2a}(s_{2a}^2-3s_{2b}^2)$	
$(333\|a_1)=s_{3x}s_{3y}s_{3z}$	$(33\|t2,x)=s_{3y}s_{3z}$
$(2222\|a_1)=(s_{2a}^2+s_{2b}^2)^2$	$(33\|t2,y)=s_{3x}s_{3z}$
$(3333\|a_1)^{(1)}=s_{3x}^4+s_{3y}^4+s_{3z}^4$	$(33\|t2,z)=s_{3x}s_{3y}$
$(3333\|a_1)^{(2)}=s_{3x}^2s_{3y}^2+s_{3x}^2s_{3z}^2+s_{3y}^2s_{3z}^2$	
$(22\|e,a)=(s_{2b}^2-s_{2a}^2)/2$	$(34\|t2,x)=(s_{3y}s_{4z}+s_{3z}s_{4y})/\sqrt{2}$
$(22\|e,b)=s_{2a}s_{2b}$	$(34\|t2,y)=(s_{3x}s_{4z}+s_{3z}s_{4x})/\sqrt{2}$
$(33\|e,a)=(2s_{3z}^2-s_{3x}^2-s_{3y}^2)/\sqrt{6}$	$(34\|t2,z)=(s_{3x}s_{4y}+s_{3y}s_{4x})/\sqrt{2}$
$(33\|e,b)=(s_{3x}^2-s_{3y}^2)/\sqrt{2}$	
$(34\|e,a)=(2s_{3z}s_{4z}-s_{3x}s_{4x}-s_{3y}s_{4y})/\sqrt{6}$	
$(34\|e,b)=(s_{3x}s_{4x}-s_{3y}s_{4y})/\sqrt{2}$	

study the potential energy surface for the CH_4^+ ion.[14,15] This section gives the form of the three-valued potential energy surface.

The coordinate system used to describe the molecule is chosen so that the coordinates of the atoms at the ground state equilibrium geometry are given by C(0,0,0), $H_1(-a,-a,a)$, $H_2(a,a,a)$, $H_3(-a,a,-a)$, and $H_4(a,-a,-a)$, where $a \equiv r_e/\sqrt{3}$ (r_e is the equilibrium C–H bond distance). Let ψ_x, ψ_y, and ψ_z be the three degenerate eigenfunctions of the Schrödinger equation for the electrons at the equilibrium geometry, where the molecule has point group T_d symmetry. The electronic wave functions transform as the T_2 irreducible representation (irrep), and transform as x, y, and z under the symmetry operations of the T_d point group. For nonsymmetric nuclear geometries, the degeneracy is lifted. Thus, there will be three adiabatic potential energy surfaces that intersect at tetrahedral geometries. Close to the equilibrium geometry the adiabatic electronic wave functions may be written as a linear combinations of ψ_x, ψ_y, and ψ_z. The wave functions $\psi_i(q)$ only depend on the electron coordinates q and not on nuclear coordinates Q and can be considered as diabatic wave functions. From group theory it follows that the matrix elements of the electronic Hamiltonian in this basis, $\langle\psi_i|\hat{H}^{\mathrm{el}}|\psi_j\rangle$, can be written as[14]

$$\begin{pmatrix} V_{a_1}-\frac{1}{2}V_{e,a}+\frac{1}{2}\sqrt{3}V_{e,b} & V_{t2,z} & V_{t2,y} \\ V_{t2,z} & V_{a_1}-\frac{1}{2}V_{e,a}-\frac{1}{2}\sqrt{3}V_{e,b} & V_{t2,x} \\ V_{t2,y} & V_{t2,x} & V_{a_1}+V_{e,a} \end{pmatrix}, \tag{1}$$

where V_{a_1}, $V_{e,i}$ $(i=a,b)$, and $V_{t2,i}$ $(i=x,y,z)$ are functions of the nuclear coordinates that transform according to irreps A_1, E, and T_2, respectively. V_{a_1} transforms as $(x^2+y^2+z^2)$ under the symmetry operations of T_d point group. The functions $V_{e,a}$ and $V_{e,b}$ transform as the pair $((2z^2-x^2-y^2)/\sqrt{6}, (x^2-y^2)/\sqrt{2})$, and the functions $V_{t2,i}$ as the set (x,y,z). V_{a_1}, $V_{e,i}$, and $V_{t_2,i}$ are expanded in powers of the symmetry-adapted internal coordinates, which are linear combinations of C–H_i bond lengths r_i and H_i–C–H_j bond angles α_{ij},

$$\begin{aligned}
s_1\ (a_1) &= \tfrac{1}{2}(r_1+r_2+r_3+r_4)-2r_e,\\
s_{2a}\ (e,a) &= (1/2\sqrt{3})(2\alpha_{12}+2\alpha_{34}-\alpha_{13}-\alpha_{14}-\alpha_{23}-\alpha_{24}),\\
s_{2b}\ (e,b) &= \tfrac{1}{2}(\alpha_{13}-\alpha_{14}-\alpha_{23}+\alpha_{24}),\\
s_{3x}\ (t_2,x) &= (1/\sqrt{2})(\alpha_{24}-\alpha_{13}),\\
s_{3y}\ (t_2,y) &= (1/\sqrt{2})(\alpha_{23}-\alpha_{14}),\\
s_{3z}\ (t_2,z) &= (1/\sqrt{2})(\alpha_{12}-\alpha_{34}),\\
s_{4x}\ (t_2,x) &= \tfrac{1}{2}(r_2+r_4-r_1-r_3),\\
s_{4y}\ (t_2,y) &= \tfrac{1}{2}(r_2+r_3-r_1-r_4),\\
s_{4z}\ (t_2,z) &= \tfrac{1}{2}(r_1+r_2-r_3-r_4).
\end{aligned} \tag{2}$$

Since these internal coordinates and potential energy terms in Eq. (1) have the same transformation properties, the zeroth and first order terms in the expanded potential are given by

$$\begin{aligned}
V_{a_1}^{(0)} &= V^{\mathrm{vert}},\\
V_{a_1}^{(1)} &= l_1 s_1,\\
V_{e,i}^{(1)} &= l_2 s_{2i} \quad (i=a,b),\\
V_{t_2,i}^{(1)} &= l_3 s_{3i} + l_4 s_{4i} \quad (i=x,y,z),
\end{aligned} \tag{3}$$

where V^{vert} is the vertical excitation energy and l_i is the expansion coefficients.

The second order terms are more complex. Direct products of internal coordinates of E or T_2 symmetry do not transform as irreps. However, the second order contributions can be expressed in terms of symmetry-adapted functions of the coordinates.[14] These functions can be found by considering the effect of permutations of the hydrogen atoms on the products of internal coordinates, and by constructing linear combinations that transform as the different irreps of T_d. Using the functions defined in Table I, the second order terms can be written as

$$\begin{aligned}
V_{a_1}^{(2)} &= \tfrac{1}{2}f_{11}s_1^2+\tfrac{1}{2}f_{22}(22|a_1)+\tfrac{1}{2}f_{33}(33|a_1)+f_{34}(34|a_1)\\
&\quad +\tfrac{1}{2}f_{44}(44|a_1),\\
V_{e,i}^{(2)} &= l_{12}s_1s_{2i}+l_{22}(22|e_i)+l_{33}^e(33|e_i)+l_{34}^e(34|e_i)\\
&\quad +l_{44}^e(44|e_i) \quad (i=a,b),\\
V_{t_2,i}^{(2)} &= l_{13}s_1s_{3i}+l_{14}s_1s_{4i}+l_{23}(23|t_2,i)+l_{24}(24|t_2,i)\\
&\quad +l_{33}^t(33|t_2,i)+l_{34}^t(34|t_2,i)+l_{44}^t(44|t_2,i)\\
&\quad (i=x,y,z).
\end{aligned} \tag{4}$$

Some cubic and quartic terms of V_{a_1} are added. The quartic terms prevent the energy to become very low for large displacements from the equilibrium geometry. The third and fourth order terms included are

$$H_{a_1}^{(3)} = \tfrac{1}{6} f_{111} s_1^3 + \tfrac{1}{6} f_{222}(222|a_1) + f_{333}(333|a_1) + f_{444}(444|a_1),$$

$$H_{a_1}^{(4)} = \tfrac{1}{24} f_{1111} s_1^4 + \tfrac{1}{24} f_{2222}(2222|a_1) + \tfrac{1}{24} f_{3333}^{(1)}(3333|a_1)^{(1)} + \tfrac{1}{4} f_{3333}^{(2)}(3333|a_1)^{(2)} + \tfrac{1}{24} f_{4444}^{(1)}(4444|a_1)^{(1)} + \tfrac{1}{4} f_{4444}^{(2)}(4444|a_1)^{(2)}. \quad (5)$$

III. METHODS

A. Electronic structure calculations

The adiabatic potential energies of the four lowest singlet states (S_0, S_1, S_2, and S_3) are calculated using the multireference single and double excitation configuration interaction (MRSD-CI) approach, employing the COLUMBUS package.[22–25] Details are the same as in Ref. 7. The molecular orbitals used to construct the reference space are based on multiconfiguration self-consistent field (MCSCF) calculations. The MCSCF calculations are state averaged over the ground state and the first three excited singlet states, with a weight of 3 for the ground state and a weight of 1 for each excited state. The 1*s* orbital is not correlated. The atomic orbital basis set employed is based on Dunnings correlation consistent polarized valence triple-zeta basis (cc-pVTZ).[26] The highest angular momentum basis functions (*f* on C and *d* on H) are omitted from the cc-pVTZ basis to reduce the computational effort. Diffuse functions for C have been added to describe the Rydberg *s* orbital: two *s* functions (exponents 0.023 and 0.007) and one *p* function (exponent 0.021). This basis set is abbreviated as "TZ$^-$/Ry" in this paper. In Ref. 7, it was shown that this basis set gives reasonable results for the first excited state.[7] In Sec. IV A, the effect of the basis set size on the absorption spectrum is examined.

B. Determination of the parameters of the potential energy surface

The first step in the present study is the determination of the parameters of the potential energy surface. Close to the reference geometry, the adiabatic potential energy surfaces obtained from the electronic structure calculations depend on the coordinates as the energy surfaces obtained by diagonalizing the matrix in Eq. (1). The parameters can be determined from the *ab initio* adiabatic energies for the first three excited states, V_1, V_2 and V_3. From Eq. (1), it follows that the average of the three adiabatic energies, $V_{\mathrm{av}} \equiv 1/3(V_1+V_2+V_3)$, only depends on V_{a_1}. On the other hand, the differences $\Delta_i \equiv V_i - V_{\mathrm{av}}$ only depend on $V_{e,i}$ and $V_{t_2,i}$. Thus, the parameters for V_{a_1}, $V_{e,i}$, and $V_{t_2,i}$ can be determined independently.

To determine the parameters, adiabatic potential energies are computed for several one and two dimensional grids. All geometries have at least C_s symmetry. The electronic structure calculations are therefore performed in C_s symmetry. The grids are chosen according to two criteria. First, the grid points lie sufficiently close to the reference geometry so that the model potential energy surface can accurately describe the *ab initio* energies. The difference between the fit and *ab initio* energies was typically about 0.1 meV. Second, the number of grid points is at least four times the number of parameters to be determined independently. It has been checked that the parameters are not changed significantly when more points are added to the grid. Table II gives the resulting parameters.

TABLE II. Parameters for the three-valued potential energy surface at r_e =2.057 bohr, for interpolation in internal coordinates. Energies in eV, bond distances in bohr, and bond angles in radians.

V^{vert}	10.5439	l_1	−1.8492
f_{11}	9.5685	l_2	−2.9994
f_{22}	2.9580	l_3	1.9289
f_{33}	2.5475	l_4	−1.5654
f_{44}	9.1831	l_{12}	1.1471
f_{34}	0.1747	l_{13}	−0.5392
f_{111}	−14.9676	l_{14}	0.3895
f_{1111}	16.6781	l_{22}	−0.0276
f_{222}	0.2163	l_{23}	−1.0208
f_{2222}	0.0000	l_{24}	−0.4599
f_{333}	−1.3841	l'_{33}	1.1078
$f_{3333}^{(1)}$	3.6754	l''_{33}	−0.0703
$f_{3333}^{(2)}$	2.5575	l'_{34}	0.7308
f_{444}	−15.0038	l''_{34}	−0.3553
$f_{4444}^{(1)}$	19.6578	l'_{44}	−0.3711
$f_{4444}^{(2)}$	19.2372	l''_{44}	0.0178

Alternatively, the potential can be expanded in Cartesian normal mode coordinates $Q_1(a_1)$, $Q_2(e)$, $Q_3(t_2)$, and $Q_4(t_2)$. The corresponding expressions are similar to Eqs. (3)–(5) (the symbols *s* should be replaced by *Q*). Close to the reference geometry, expansion in Cartesian normal mode coordinates yields the same potential energy surfaces as expansion in the curvilinear internal coordinates. However, for a truncated power expansion, it will give different results for large displacements from the equilibrium geometry. It is *a priori* not clear which of the expansions, in internal or normal mode coordinates, gives a better representation of the potential energy surfaces. In this paper, the absorption spectrum will be calculated for both expansions to examine the effect of the expansion of the calculated absorption spectrum. The expansion coefficients for the normal mode representation can be determined following the same procedure as used to determined the coefficients for the expansion in internal coordinates.

C. Quantum dynamics calculations

Once the parameters of the potential energy surface are determined, electronically nonadiabatic quantum dynamics simulations can be performed to calculate the cross section. The photodissociation cross section σ for randomly oriented molecules can be written as[27,28]

$$\sigma(E_{\mathrm{ph}}) = \frac{1}{3}\frac{1}{2\hbar^2 c \epsilon_0} E_{\mathrm{ph}} \int_{-\infty}^{\infty} dt \exp(\mathrm{i}Et/\hbar) S(t), \quad (6)$$

where c is the velocity of light, ϵ_0 is the permittivity of free space, E_{ph} is the photon energy, E is the total energy, and $S(t)$

TABLE III. Force constants for the ground state potential energy surface at r_e=2.057 bohr and normal mode frequencies. Energies in eV, bond distances in bohr, and bond angles in radians.

f_{11}	9.5613	$\omega_1(a_1)$	3035 cm^{-1}
f_{22}	3.6338	$\omega_2(e)$	1575 cm^{-1}
f_{33}	3.4027	$\omega_3(t_2)$	1360 cm^{-1}
f_{44}	9.3183	$\omega_4(t_2)$	3143 cm^{-1}
f_{34}	0.7120		

is the so-called "autocorrelation function." The autocorrelation function is defined as

$$S(t) = \langle \Psi_0 | \exp(-i\hat{H}t/\hbar) | \Psi_0 \rangle, \tag{7}$$

where $\hat{H}$ is the excited state Hamiltonian, and Ψ_0 is the initial wave function. Ψ_0 is given by

$$\Psi_0(q,Q) = \mu(Q)\chi(Q)\psi_{\text{exc}}(q), \tag{8}$$

where q and Q represent electron and nuclear coordinates, respectively, $\mu(Q)$ is the transition dipole moment, $\chi(Q)$ is the ground state vibrational wave function, and $\psi_{\text{exc}}(q)$ is the wave function for the excited electronic state. In the present work, the excited electronic state is ψ_z. The cross sections for excitation to the ψ_x and ψ_y states are equal to the cross section for excitation to the ψ_z state. Thus, the total cross section can be obtained by multiplying the cross section for excitation to the ψ_z state with three.

The calculation of the autocorrelation function requires the propagation of wave packets on coupled electronic states. The MCTDH method[17–20] is employed for efficient multidimensional wave packet propagation. MCTDH is a time-dependent wave packet approach employing time-dependent basis functions, called "single-particle functions," to represent the wave function. This allows for a very compact representation of the wave function. The correlation discrete variable representation (CDVR) method[29,30] is employed to calculate matrix elements of the potential energy operator in the basis of single-particle functions.

The wave function is represented in the diabatic representation of the electronic states. Nuclear coordinates are normal mode coordinates, and vibrational angular momentum terms are neglected. The normal mode coordinates are based on the force constants for the ground state, obtained similarly as the parameters for the excited state. The force constants and harmonic frequencies for the ground state are listed in Table III.

The ground state vibrational wave function $\chi(Q)$ is evaluated using the harmonic approximation. The coordinate dependence of the transition dipole moment μ has been neglected. The constant value of μ has been adjusted to obtain the best possible agreement with experiment. The obtained value of μ is 0.732 a.u., slightly larger than the result of *ab initio* calculations at the ground state equilibrium geometry (0.668 a.u.).[7]

Convergence of the MCTDH calculations has been carefully checked. More details are given in Sec. IV B. Table IV gives the parameters for the converged calculations. Each set of single-particle functions is represented using a Hermite DVR.

TABLE IV. Parameters for the MCTDH representation of the wave function. The number of grid points in parenthesis corresponds to the long time propagation (16 fs).

Coordinate		Number of single-particle functions	Number of grid points	
Q_1	(a_1)	2	30	(100)
Q_{2a}	(e,a)	5	55	(100)
Q_{2b}	(e,b)	5	35	(65)
Q_{3x}/Q_{3y}	(t_2,i)	6	40	(100)
Q_{3z}	(t_2,z)	3	25	(45)
Q_{4x}/Q_{4y}	(t_2,i)	3	20	(50)
Q_{4z}	(t_2,z)	2	20	(30)

IV. RESULTS

A. Potential energy surfaces

The potential energy surfaces are constructed so that they fit the *ab initio* adiabatic energies very accurately close to the ground state equilibrium geometry. However, at larger displacements the fit starts to deviate significantly from the results of the electronic structure calculations. This is mainly because the electronic wave functions can no longer be approximated by linear combinations of ψ_x, ψ_y, and ψ_z. Other electronic states, also with different symmetry species, should be included. Figure 1 presents a cut through the potential energy surface as a function of the normal mode coordinates along the line $Q_{2a}=Q_{3z}$. Modes $Q_2(e)$ and $Q_3(t_2)$ are predominantly H–C–H bending modes. Along the line $Q_{2a}=Q_{3z}$, the splitting of adiabatic energies is quite strong due to the cooperation of the H_{t_2z} and $H_{e,a}$ couplings. In the range between −10 and 10 a.u., where the bond angles differ by less than 15° from the equilibrium values, the fitted surface perfectly reproduces the computed energies, but for larger displacements the fit and the calculated energies diverge. The V_2 and V_3 surfaces have avoided crossings due to the mixing of configurations with excitation to Rydberg 3*s* and 3*p* orbitals. The fitted surface, on the other hand, can

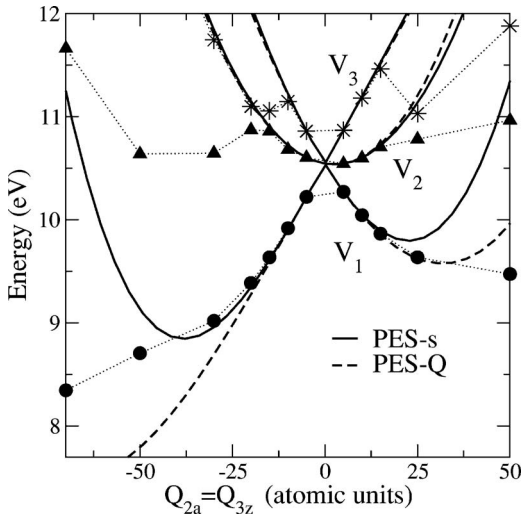

FIG. 1. Adiabatic potential energy surfaces, obtained from the fit in internal coordinates ("PES-s") and Cartesian normal mode coordinates ("PES-Q"), as a function of normal modes $Q_{2a}=Q_{3z}$. The circles, triangles, and stars are the *ab initio* adiabatic energies V_1, V_2, and V_3, respectively.

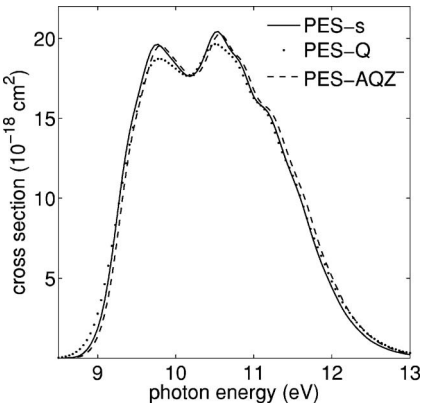

FIG. 2. Cross section for potential energy surfaces PES-s, PES-Q, and PES-AQZ⁻. PES-AQZ⁻ is constructed as PES-s, but is based on calculations with the AQZ⁻/Ry basis set and with 1*s* core correlation.

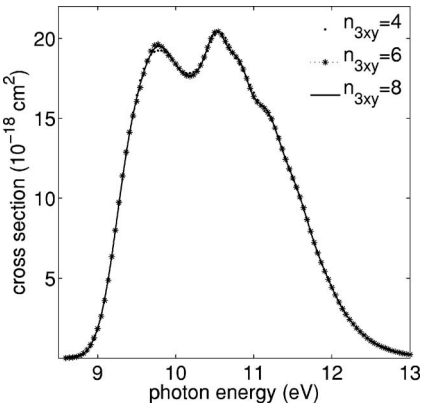

FIG. 3. Convergence of the cross section with the number of single-particle functions for modes Q_{3x} and Q_{3y}. The number of single-particle functions for the other modes is given in Table IV.

only represent the potential energy surfaces for electronic states resulting from the $1t_2 \rightarrow 3s$ transition.

Figure 1 also shows the potential energy surfaces obtained from expansion in Cartesian normal mode coordinates. The two sets of potential energy surfaces are referred to as "PES-s" and "PES-Q," where *s* and *Q* stand for the curvilinear internal and Cartesian normal mode coordinates, respectively. For the lowest adiabatic energy surface V_1, the decrease in energy is significantly stronger for PES-Q than for PES-s. This is found also in other cuts through the potential energy surface. The *ab initio* points appear to lie in the middle between the two potential energy surfaces.

Thus, we have two sets of potential energy surfaces, PES-s and PES-Q, which both accurately describe the *ab initio* data close to the reference geometry, but deviate substantially at larger displacements. However, we may assume that the cross section is mainly determined by the potential energy surface in the Franck-Condon region. By comparing cross sections calculated using the two potential energy surfaces, this assumption can be verified. Figure 2 shows that the differences between the two spectra are small. PES-Q only gives a somewhat broader spectrum.

It is also useful to examine the accuracy of the electronic structure calculations. In a previous study Ref. 7, it was shown that the vertical excitation energy increases when the basis set is increased to augmented valence quadruple zeta level, and when 1*s* core correlation is included. To study the effect of the basis set size and of the core correlation, the parameters are also determined from electronic structure calculations with the "AQZ⁻/Ry" basis set[7] and with 1*s* core correlation. The AQZ⁻/Ry basis set is obtained from the TZ⁻/Ry basis set by replacing the valence triple zeta basis functions with the augmented valence quadruple zeta basis set. The highest orbital angular momenta (*g* on C, *f* on H) are then removed. The electronic structure calculations are repeated with the larger basis set, using the same grids as before. However, because these calculations are expensive when performed in C_s symmetry, we have only repeated the calculations for the C_{2v} cuts of coordinate space. All parameters except f_{333}, $f^{(2)}_{3333}$, f_{444}, $f^{(2)}_{4444}$, l^t_{33}, l^t_{44}, and l^t_{34} can be determined in C_{2v} symmetry. For the parameters that could not be calculated, we took the TZ⁻/Ry results. The basis set size and core correlation have a significant effect on V^{vert}, which increases from 10.54 to 10.59 eV, but have a small effect on the other parameters. Figure 2 shows that the spectrum obtained from more accurate electronic structure calculations is close to the TZ⁻ result. The main effect is that the spectrum is shifted to higher energies by about 0.05 eV.

B. Convergence of the MCTDH calculations

In this section, the convergence of the MCTDH calculations with respect to basis set parameters and propagation time is discussed. The general strategy to determine the number of single-particle functions is the same as used by Manthe and co-workers in their studies on the $H+CH_4$ reaction.[31–34] After some exploratory calculations, a first trial set of single-particle functions was constructed. This set contains one single-particle function for Q_1, four for Q_{2a}/Q_{2b}, four for Q_{3x}/Q_{3y}, two for Q_{3z}, two for Q_{4x}/Q_{4y}, and one for Q_{4z}. This set already gives a reasonable result for the cross section. Mode Q_{3z} requires much less single-particle functions than modes Q_{3x} and Q_{3y}. This can be explained as follows. At $t=0$, only the ψ_z state is populated. Equations (1)–(4) show that the off-diagonal coupling between the ψ_z state and the ψ_x and ψ_y states depends on the *x* and *y* components of Q_3 and Q_4, but not on the *z* components. Thus, the *x* and *y* components of the t_2 modes are much more strongly excited than the *z* components.

For each mode, the number of single-particle functions is varied independently to achieve convergence. The final set is listed in Table IV. The convergence is then checked again by varying the number of single-particle functions starting from the final set. As an example of convergence, we show in Fig. 3 the convergence with respect to the number of single-particle functions in Q_{3x} and Q_{3y}, n_{3xy} (because of symmetry, we always use the same number of single-particle functions for the *x* and *y* components of Q_3 and Q_4). The $n_{3xy}=6$ and $n_{3xy}=8$ results are almost indistinguishable, while small differences between the $n_{3xy}=4$ and $n_{3xy}=6$ results are visible.

All convergences tests are based on a propagation time of 8 fs, giving an autocorrelation function $[S(t) = \langle \Psi(-t/2) | \Psi(t/2) \rangle]$ for times up to 16 fs. The choice of

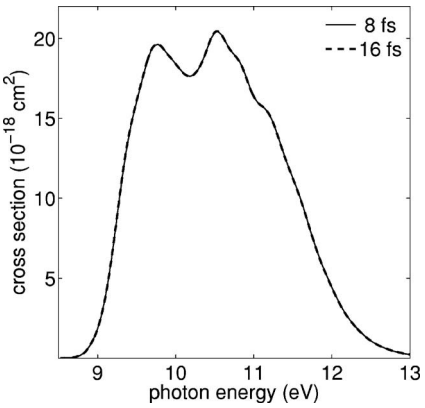

FIG. 4. Convergence of the cross section with the propagation time.

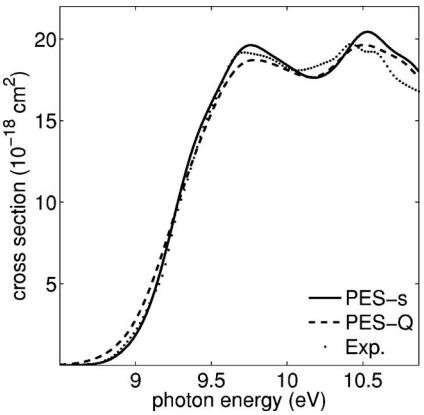

FIG. 5. Comparison of the calculated cross sections, obtained with the two potential energy surfaces, with experimental data of Ref. 1.

8 fs for the time propagation is not arbitrarily. At 16 fs, $S(t)$ has decreased to almost zero ($|S(16\ \text{fs})| \approx 10^{-4}|S(0)|$). A calculation with a longer propagation time (16 fs) shows that $|S(t)|$ does not increase significantly for at least another 8 fs. For the 16 fs propagation, we used the same number of single-particle functions as for the 8 fs propagation, but the number of DVR grid points to represent each single-particle function is increased significantly (see Table IV). Convergence tests for the number of single-particle functions have not been repeated for the longer propagation time. Figure 4 compares the cross sections obtained from the 8 and 16 fs time propagation calculations. The two results are almost identical. Thus, the cross section is independent of the propagation time between 8 and 16 fs.

Although the cross section appears to be converged with respect to the propagation time, it cannot be the exact solution for the PES model. The potential energy surfaces are not dissociative and only support bond states. The exact spectrum for infinite propagation time should therefore be a stick spectrum. For longer propagation times, one would expect to see some vibrational structures in the spectrum. However, several test calculations suggest that it is difficult to obtain convergence of the MCTDH/CDVR calculations with respect to the number of single-particle functions after 8 fs. This is probably due to the high density of vibrational levels, resulting from the strong Jahn-Teller distortion for the Q_2 and Q_3 modes. Thus, the present dynamical calculations can only accurately describe the short time dynamics. Also the PES model is only accurate close to the equilibrium geometry, and is therefore only valid for the short time dynamics after photoexcitation.

C. Cross sections for CH_4 and CD_4: Comparison with experiment

The cross sections calculated using PES-s and PES-Q are compared with the experimental cross section in Fig. 5. Only energies up to 10.85 eV are considered. For higher energies the bands due to the $1t_2 \rightarrow 3s$ and $1t_2 \rightarrow 3p$ transitions overlap in the experimental spectrum. The calculated result is in good agreement with experiment. The two peaks are reproduced in the calculations, with about the same spacing as in experiment. The difference between experiment and theory is comparable to the difference between the PES-s and PES-Q results. Both the calculated and the experimental spectrum are diffuse and do not show clear vibrational progressions. However, this is for different reasons. In the experiment, methane dissociates into various fragments.[1,8–11] This explains the short lifetime of the excited state, and the absence of clear vibrational progressions, although some irregularities in the experimental spectrum around 10.5 eV could be a signature of resonances. The present calculations only describe the dynamics within the first 8 fs (see Sec. IV C) and therefore yield a diffuse spectrum without vibrational structures.

The theoretical cross sections is purely based on *ab initio* calculations with exception of the transition dipole moment, which has been adjusted to obtain best possible agreement with experiment. The value found in this way, $\mu = 0.732$ a.u., is a factor of 1.095 larger than the *ab initio* value of 0.668 a.u.[7] Larger basis sets and core correlation[7] have little effect on the calculated μ. We have also checked that the coordinate dependence of μ cannot explain the discrepancy. *Ab initio* calculations of the transition dipole moment at several cuts through coordinate space show that μ depends weakly on the nuclear coordinates in the Franck-Condon region. The disagreement with experiment is probably due to a truncation of the CI expansion in Ref. 7. Scaling of the transition dipole moment was also necessary in a study of the first absorption band of water.[35] In that work, the *ab initio* transition dipole moment was found to be about 10% too large. Thus, it appears that the typical uncertainty in transition dipole moments calculated with the MRSD-CI method is about 10%.

To further test the accuracy of the potential energy surface and the adjusted transition dipole moment, it would be useful if accurate experimental cross sections for CD_4 were available. The predicted spectrum, shown in Fig. 6, is significantly narrower than the spectrum for CH_4. The CD_4 calculations are converged with the same number of single-particle functions as the CH_4 calculations.

V. DISCUSSION

In the previous section, the accuracy of the computational approach has been discussed in detail. The comparison with experiment also suggests that the present *ab initio* treat-

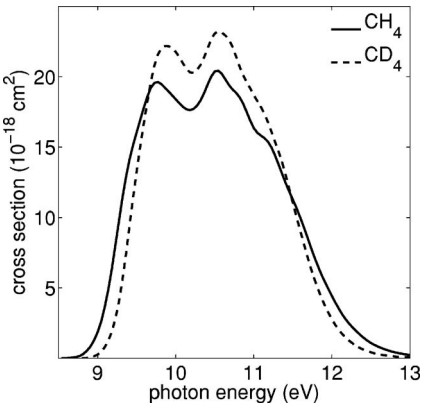

FIG. 6. The isotope effect on the absorption spectrum of methane.

ment is realistic. In this section, the structure of the spectrum is examined in more detail. To gain insight, we will use the same semiclassical reflection approach as used by Dixon[14] in his study of the photoelectron spectrum of methane.

The photoelectron spectrum[16] has a similar shape as the photodissociation spectrum. This is not surprising. In the Franck-Condon region, the $1\,^2T_2$ state of CH_4^+ is similar to the $1\,^1T_2$ Rydberg state of CH_4. Dixon[14] has examined the structure of the photoelectron spectrum using the reflection approximation. According to this semiclassical model, the peaks correspond to different adiabatic potential energy surfaces, V_1, V_2, and V_3, that become degenerate at tetrahedral geometries. This model can similarly explain the features in the absorption spectrum.

According to the semiclassical reflection approximation, the cross section is determined by a mapping of the ground state vibrational wave function on the excited state potential energy surfaces. The cross section for excitation to the ith adiabatic electronic state is given by[27]

$$\sigma_i^R(E_{\rm ph}) = \frac{1}{3}\frac{\pi}{\hbar c \epsilon_0} E_{\rm ph} \int dQ\, \delta(E - V_i(Q)) |\mu(Q)|^2 |\chi(Q)|^2, \tag{9}$$

where $V_i(Q)$ is the potential energy surface for the ith adiabatic electronic state and $\mu_i(Q)$ is the transition dipole moment. In the present case, μ_i is assumed to be a constant. To evaluate Eq. (9), a Monte Carlo sampling scheme has been applied. Nuclear coordinates Q are selected at random according to the probability $|\chi(Q)|^2$. From the distribution of potential energies, the cross section can be calculated.

Figure 7 presents the results of the reflection approximation calculations, both the individual contributions of the three adiabatic potential energy surfaces V_1, V_2, and V_3, and the total cross section. For each adiabatic surface, the spectrum has a simple Gaussian shape, but the width increases with the index of the electronic state. The maxima in the V_1 and V_2 spectra coincide with the two peaks in the total spectrum. The V_3 component does not give rise to a peak in the total spectrum, because of the strong overlap between the V_2 and V_3 contributions. However, the total spectrum clearly shows a "shoulder" (a local minimum of the slope of the spectrum) around 10.8 eV, which clearly originates from the overlapping contributions of the V_2 and V_3 spectra.

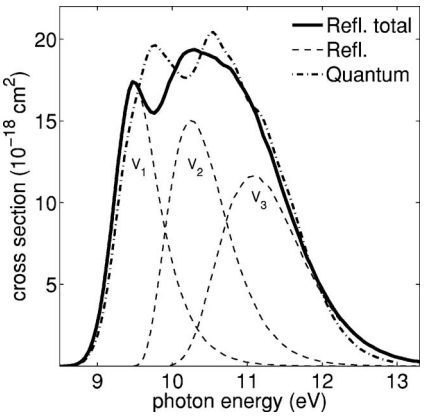

FIG. 7. Cross sections obtained from semiclassical reflection approximation calculations. Thick solid line: total spectrum. Dashed lines: contributions of the adiabatic potential energy surfaces. Also shown is the quantum result for comparison (dashed-dotted line).

In this work, the accuracy of the reflection approximation can be assessed. Figure 7 includes the quantum result for comparison. Both the semiclassical and quantum results show the presence of two clear peaks, and a shoulder at higher energies. However, for the reflection model the peaks are shifted by about 0.3 eV to lower energies. The difference is probably the consequence of neglecting the non-Born-Oppenheimer terms in the Hamiltonian in the reflection approximation (see also the discussion in Ref. 13). If the couplings $V_{t_2,i}$ are set to zero, then the diabatic ψ_z is an eigenfunction of the electronic Hamiltonian, and the results of the reflection method are in perfect agreement with the quantum result. Both no longer show a double-peak structure.

It is interesting to study the dependence on the peak-peak separation on the number of vibrational modes included in the calculations. Figure 8 presents the spectrum calculated by including only the bending modes $Q_2(e)$ and $Q_3(t_2)$ [five dimensional (5D)] and the spectrum calculated by only including mode $Q_3(t_2)$ (three dimensional). The structure in the 5D spectrum is more clear than in the full dimensional spectrum. In particular, instead of the shoulder at high energies, a third peak is clearly visible. However, the peak-peak separation is similar as in the full dimensional calculations. The omitted modes $Q_1(a_1)$ and $Q_4(t_2)$ do not play an important

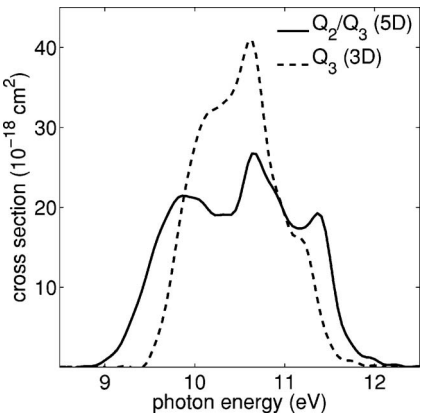

FIG. 8. Cross sections obtained from reduced dimensionality calculations.

role in the splitting of the absorption band. Mode $Q_1(a_1)$ does not cause a splitting, and the Jahn-Teller distortion for the $Q_4(t_2)$ mode is small.

When only the $Q_3(t_2)$ mode is included, then the separation between the peaks is much smaller. At first sight, this seems surprising, since the $Q_2(e)$ modes alone cannot induce a splitting of the absorption band. When the Q_3 and Q_4 are zero, then the diabatic electronic states are eigenstates of the electronic Hamiltonian. Thus, there is only one relevant potential energy surface corresponding to ψ_z, given by $V_{a_1} + V_{e,a}$, and the absorption spectrum is a single broad band. However, when both $Q_2(e)$ and $Q_3(t_2)$ modes are excited simultaneously, then the excitation of the Q_2 modes results in a significant increase of the splitting of the band.

VI. CONCLUSION

Accurate cross sections for the photodissociation of CH_4 and CD_4 are presented, based on an accurate representation of the potential energy surfaces and electronically nonadiabatic couplings around the ground state equilibrium geometry geometry, and MCTDH wave packet calculations.

The calculated spectrum is in good agreement with experiment. The two band maxima are reproduced in the calculations. We attribute these peaks to the adiabatic electronic states S_1 and S_2. According to the semiclassical reflection approximation, the peaks are maxima in the distribution of the adiabatic potential energies. In the quantum mechanical picture, these peaks correspond to maximum overlap between the ground state wave function and the continuum wave functions on the different adiabatic potential energy surfaces. Nonadiabatic couplings have a strong effect on the positions and widths of the peaks in the spectrum. Consequently, the reflection principle cannot reproduce the experimental spectrum for excitation to a degenerate electronic state. Nonadiabatic quantum calculations are required to obtain good agreement with experiment.

ACKNOWLEDGMENTS

The author thanks Professor U. Manthe for providing his MCTDH package, and Professor A. van der Avoird and Dr. G. C. Groenenboom for useful suggestions about the manuscript. The work is financially supported by the Nederlandse Organisatie voor Wetenschappelijk Onderzoek (NWO).

[1] L. C. Lee and C. C. Chiang, J. Chem. Phys. **78**, 688 (1983).
[2] S. Karplus and R. Bersohn, J. Chem. Phys. **51**, 2040 (1969).
[3] M. S. Gordon, Chem. Phys. Lett. **52**, 161 (1977).
[4] M. S. Gordon and J. W. Caldwell, J. Chem. Phys. **70**, 5503 (1979).
[5] H. U. Lee, Chem. Phys. **39**, 271 (1979).
[6] A. M. Mebel, S.-H. Lin, and C.-H. Chang, J. Chem. Phys. **106**, 2612 (1997).
[7] R. van Harrevelt, J. Chem. Phys. **125**, 124302 (2006).
[8] R. A. Brownsword, M. Hillenkamp, T. Laurent, R. K. Vasta, H.-R. Volpp, and J. Wolfrum, Chem. Phys. Lett. **266**, 259 (1997).
[9] J.-H. Wang, K. Liu, Z. Min, H. Su, R. Bersohn, J. Preses, and J. Z. Larese, J. Chem. Phys. **113**, 4146 (2000).
[10] A. H. Laufer and J. R. McNesby, J. Chem. Phys. **49**, 2272 (1968).
[11] R. E. Rebbert and P. Ausloos, J. Photochem. **1**, 171 (1972).
[12] M. G. Curtis and I. C. Walker, J. Chem. Soc., Faraday Trans. 2 **85**, 659 (1989).
[13] M. D. Sturge, Solid State Phys. **20**, 91 (1967).
[14] R. N. Dixon, Mol. Phys. **20**, 113 (1971).
[15] R. F. Frey and E. R. Davidson, J. Chem. Phys. **88**, 1775 (1988).
[16] J. W. Rabalais, T. Bergmark, L. O. Werme, L. Karlsson, and K. Siegbahn, Phys. Scr. **3**, 13 (1971).
[17] H.-D. Meyer, U. Manthe, and L. S. Cederbaum, Chem. Phys. Lett. **165**, 73 (1990).
[18] U. Manthe, H.-D. Meyer, and L. S. Cederbaum, J. Chem. Phys. **97**, 3199 (1992).
[19] M. H. Beck, A. Jäckle, G. A. Worth, and H.-D. Meyer, Phys. Rep. **324**, 1 (2000).
[20] H.-D. Meyer and G. A. Worth, Theor. Chem. Acc. **109**, 251 (2003).
[21] U. Manthe, Chem. Phys. **329**, 168 (2006).
[22] H. Lischka, R. Shepard, F. B. Brown, and I. Shavitt, Int. J. Quantum Chem., Quantum Chem. Symp. **15**, 91 (1981).
[23] R. Shepard, I. Shavitt, R. M. Pitzer, D. C. Comeau, M. Pepper, H. Lischka, P. G. Szalay, R. Ahlrichs, F. B. Brown, and J. Zhao, Int. J. Quantum Chem., Quantum Chem. Symp. **22**, 149 (1988).
[24] H. Lischka, R. Shepard, R. M. Pitzer *et al.*, Phys. Chem. Chem. Phys. **3**, 664 (2001).
[25] H. Liscka, R. Shepard, I. Shavitt *et al.*, COLUMBUS, An *ab initio* electronic structure program, Release 5.9.0, 2005.
[26] T. H. Dunning, Jr., J. Chem. Phys. **90**, 1007 (1989).
[27] E. J. Heller, J. Chem. Phys. **68**, 2066 (1978).
[28] G. G. Balint-Kurti, R. N. Dixon, and C. C. Marston, J. Chem. Soc., Faraday Trans. **86**, 1741 (1990).
[29] U. Manthe, J. Chem. Phys. **105**, 6989 (1996).
[30] A. Viel, W. Eisfeld, S. Neuman, W. Domcke, and U. Manthe, J. Chem. Phys. **124**, 214306 (2006).
[31] F. Huarte-Larranaga and U. Manthe, J. Phys. Chem. A **105**, 2522 (2001).
[32] F. Huarte-Larranaga and U. Manthe, J. Chem. Phys. **116**, 2863 (2002).
[33] T. Wu, H. J. Werner, and U. Manthe, J. Chem. Phys. **124**, 164307 (2006).
[34] T. Wu and U. Manthe, Science **306**, 2227 (2004).
[35] R. van Harrevelt and M. C. van Hemert, J. Chem. Phys. **114**, 9453 (2001).